AN X-RAY ABSORPTION STUDY OF THE IRON SITE IN BACTERIAL PHOTOSYNTHETIC REACTION CENTERS

GRANT BUNKER, EDWARD A. STERN, ROBERT E. BLANKENSHIP, AND WILLIAM W. PARSON
Departments of Physics and Biochemistry, University of Washington, Seattle, Washington 98195

ABSTRACT Measurements were made of the extended x-ray absorption fine structure (EXAFS) of the iron site in photosynthetic reaction centers from the bacterium *Rhodopseudomonas sphaeroides*. Forms with two quinones, two quinones with added *o*-phenanthroline, and one quinone were studied. Only the two forms containing two quinones maintained their integrity and were analyzed. The spectra show directly that the added *o*-phenanthroline does not chelate the iron atom. Further analysis indicates that the iron is octahedrally coordinated by nitrogen and/or oxygen atoms located at various distances, with the average value of about 2.14 Å. The analysis suggests that most of the ligands are nitrogens and that three of the nitrogen ligands belong to histidine rings. This interpretation accounts for several unusual features of the EXAFS spectrum. We speculate that the quinones are bound to the histidine rings in some manner. Qualitative features of the absorption edge spectra also are discussed and are related to the Fe–ligand distance.

I. INTRODUCTION

The primary processes in bacterial photosynthesis occur in a complex called the "reaction center," which contains protein, bacteriochlorophyll, bacteriopheophytin, two quinones, and a single iron atom. Excitation of the reaction center by light results in electron transfer from a bacteriochlorophyll complex to one of the quinones, via one or more intermediary electron carriers (1, 2). An electron moves from the first quinone to the second in about 100 μs (3, 4). The iron atom has been implicated in facilitating electron transfer between the two quinones; removal of the Fe prevents this reaction (5). The significance of this observation is unclear, however, because the conditions used to remove the iron also cause dissociation of the protein subunits of the reaction center (6). It is not known how the iron is disposed relative to the quinones. The iron chelator *o*-phenanthroline (*o*-phen) blocks electron transfer between the quinones (3, 7, 8), but it has not been clear whether this occurs as a result of iron chelation or by some other mechanism. Both quinones must be close to the iron, because there is a strong magnetic interaction between the iron and the anionic radical of either quinone (1). Nonetheless, Butler et al. (9) have shown that extraction of the quinones from reaction centers causes only minor changes in the magnetic properties of the iron. Magnetic susceptibility data (9) are consistent with the iron's being in a distorted octahedral ligand configuration. Additional information regarding ligand distances and the nature of the ligands has not been available.

To obtain information on the iron site in reaction centers, we have used extended x-ray absorption fine structure (EXAFS) spectroscopy. The EXAFS technique uses an atom's own electrons as a probe of the local environment (10–15). By using x rays of appropriate energy one can excite an electron from the 1s state[1] of a selected atomic species to an unbound propagating state. The wavelength of the outgoing electron can be varied by changing the energy of the exciting x ray. The electron wave is scattered by the atoms surrounding the absorbing atom, so that the outgoing and backscattered waves interfere near the nucleus of the absorbing atom, where the 1s state is localized. As one changes the x-ray energy and thus the photoelectron wavelength, the interference varies between constructive and destructive. This manifests itself in modulations in the x-ray absorption coefficient as a function of energy. These may be interpreted to characterize the local environment of the absorbing atom, yielding information about the coordination number, the types of neighbors, and the degree of disorder.

In its simplest form, the fractional change in atomic absorption coefficient μ that is induced by the presence of neighboring atoms can be expressed by (10–16)

$$(\mu - \mu_0)/\mu_0 \equiv \chi(k) = \sum_j \frac{N_j B_j(k)}{r_j^2} \exp(-2r_j/\lambda)\sin[2kr_j + \delta_j(k)] \times \exp(-2k^2\sigma_j^2). \quad (1)$$

Dr. Blankenship's present address is the Department of Chemistry, Amherst College, Amherst, Mass.

[1]We deal only with K-edge EXAFS in this paper.

Here μ_0 is the atomic absorption coefficient of an isolated atom and is a smoothly varying function of energy. The sum is over coordination shells at distances r_j. A coordination shell consists of N_j similar atoms at the average distance r_j, and σ_j is the root-mean-square variation of their distances about the average. The distances to individual atoms in a given coordination shell may differ due to thermal motion or structural disorder. The electron wave number k is defined by $\hbar^2k^2/2m = (E - E_0)$, where E is the photon energy, and E_0 and m are the binding energy and mass of the electron. The functions $B(k)$ and $\delta(k)$ include, respectively, the backward scattering amplitude and the phase shift, which both depend on the type of backscatterer, and λ is a phenomenological mean-free-path term that is intended to account for the finite lifetime of the propagating state and is generally a function of k. $B(k)$ and $\delta(k)$ also include contributions from the absorbing atom.

It is possible to extract r_j and σ_j from the EXAFS spectrum by the "ratio method," in which one compares the sample of interest with a suitable standard (12). The EXAFS due to a given coordination shell (j) is isolated by Fourier filtering, and its phase and amplitude are determined as functions of k for both the sample and the standard. If the backscattering atoms are of the same type in both (and certain criteria are satisfied as discussed below), the phase difference will be $2k(r_2 - r_1)$, where r_2 and r_1 are the distances to the coordination shells in the sample and the standard. A plot of the phase difference vs. k will then extrapolate to zero at $k = 0$. Similarly, a plot of the logarithm of the ratio of the amplitudes vs. k^2 will yield a straight line of slope equal to twice the difference in σ^2 and an intercept of $\ln(N_1r_2^2/N_2r_1^2)$ at $k = 0$. If the backscattering atoms are not the same, or σ is not small enough for the form of Eq. 1 to be valid, the phase difference and amplitude ratio will generally have a more complicated variation with k.

II. EXPERIMENTAL

Data were taken during several runs at the Stanford Synchrotron Radiation Laboratory (SSRL) using beam lines I, II in its original form, and IV (the wiggler line). The data that were acquired during different runs, with different samples, and different beam lines were mutually consistent, although the quality improved substantially in later measurements when a filter assembly (17) was added to the fluorescence apparatus. The best signal-to-noise ratio was obtained by measuring the reaction centers in a fluorescence mode (18) and the model compounds in a transmission mode. The iron in the reaction center samples was so dilute (~2.8 mM) that no usable spectra were obtainable in the transmission mode. Most of the results presented in this paper are based on sums of 13 scans on the G.-Feher sample described below, with total statistics of about 7×10^6 photons per data point. The signal from the iron k-edge was about half as large as that of the background, so that the effective number of counts if no background were present was about 2×10^6 per data point. The summed spectrum is presented in Fig. 1*a*.

We used a silicon (111) crystal monochromator in all but two cases, when a germanium (111) crystal or a silicon (220) was used. The monochromator was detuned routinely when possible to reduce contamination from harmonics. The energy resolution was better than 3 eV (according to the 10–90% criterion) in all cases. All of the data suffer from monochromator glitches, which are in part due to undesired reflections in the monochromator crystal. Glitches are a property of the crystal type, occurring reproducibly at a given energy, and they are usually clearly distinguishable from real data. The only serious glitches occurred at $\sim k = 8.5$ Å^{-1}, above which the EXAFS signal from reaction centers became too small to be useful.

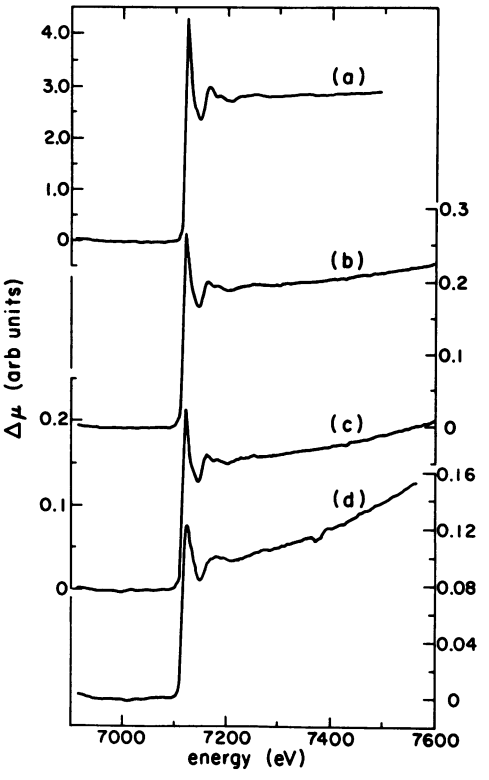

FIGURE 1 The K-edge x-ray absorption spectrum of the Fe in reaction centers. (*a*) The spectrum of a two-quinone sample with added *o*-phen supplied by G. Feher. (*b*) The spectrum of a two-quinone sample prepared in our laboratory. (*c*) The spectrum of a two-quinone sample with added *o*-phen prepared in our laboratory. (*d*) The spectrum of a one-quinone sample which was found to have degraded. Arbitrary (arb) units.

Reaction center samples were prepared independently in two laboratories. Reaction centers containing close to two quinones per particle (2Q) were prepared from *Rhodopseudomonas sphaeroides* strain R-26, as described previously (5). The Fe content was measured by atomic absorption to be 0.7 equivalents/mol of reaction centers. Reaction centers containing one quinone (1Q) were obtained from the 2Q reaction centers as described by Okamura et al. (19). The reaction centers were concentrated to a runny paste by pressure dialysis and placed in Plexiglas cells with Kapton (DuPont Instruments, Wilmington, DE) windows. 10 mM *o*-phen was added to some of the samples before they were concentrated. All measurements were performed at room temperature. Optical absorption spectra of diluted samples were measured before and after the experiment. Degradation of the reaction centers was monitored by the conversion of their bacteriochlorophyll to bacteriopheophytin. We found only slight degradation (<10%) of the 2Q and *o*-phen-treated samples. As no change was observed in the EXAFS spectra during the course of the experiment, we infer that no significant degradation of these samples occurred during the measurements. The 1Q sample unfortunately showed sufficient degradation that we could not trust its spectra as

TABLE I
RELEVANT PROPERTIES OF THE STANDARDS USED FOR EXAFS ANALYSIS

Standard	Designation in text	Coordination number N	Mean first-neighbor distance	Variation in first-neighbor distances
			$\bar{R}$(Å)	σ^2(Å^2)
Bis(acetonitrile)-(2,3,9,10-tetramethyl-1,4,8,11-tetraaza-cyclotetradeca-1,3,8,10-tetranene) iron(II) hexafluorophosphate	iron-TIM	6 nitrogen	1.94	0.0001
Tris(*o*-phenanthroline)iron (III) perchlorate hydrate	iron-*o*-phen	6 nitrogen	1.97	0.0001
Tri-μ_3-oxo-triaquo-hexakis (glycine) triiron (III) perchlorate	iron-glycine	6 oxygen	2.02	0.0031
Ferrous oxalate dihydrate	iron-oxalate	6 oxygen	2.12	0.0011

accurately depicting an intact 1Q sample. Fig. 1*d* shows this suspect 1Q spectrum, which is substantially different from the 2Q spectrum. In particular, the peak at the edge is broadened and decreased in amplitude.

Reaction centers from *Rps. sphaeroides* R-26 with added *o*-phen were independently prepared by the method of Feher and Okamura (1) and were suspended in a polyvinyl alcohol film, which was folded and placed in a polyethylene holder. The holder was hermetically sealed because of the hygroscopic nature of the film. The sample was kindly supplied by George Feher (University of California at San Diego).

The iron glycine standard tri-μ_3-triaquo-hexakis(glycine)-triiron(III) perchlorate was prepared according to the methods of Tucker et al. (20) and was supplied by Elizabeth Holt (University of Wyoming). Its structure is known from the work of Thundathil et al. (21). The compound bis(acetonitrile)-(2,3,9,10-tetramethyl-1,4,8,11-tetraazacyclotetradeca-1,3,8,10-tetraene)iron(II) hexafluorophosphate (iron-TIM) was characterized and supplied by Norman Rose (University of Washington). Iron(II)-*o*-phen and iron(III)-*o*-phen were prepared by methods described previously (22, 23). Fe(III) acetylacetonate and Fe(II) oxalate dihydrate (humboldine) were obtained from Research Organic/Inorganics Chemical Corp (Sun Valley, Ca) and Matheson, Coleman, Bell (Norwood, Ohio), respectively. Their structures are found in Wyckoff (24). All of the models have either all-nitrogen or all-oxygen first neighbors in an octahedral arrangement. All are stable under laboratory conditions. Fe(III) acetylacetonate proved unsatisfactory as a standard, because its EXAFS spectrum indicated that it was heteromorphous. In a past analysis (5), a careful comparison of the first shell EXAFS had been made between the glycine standard and an α-FeOOH standard showing good transferability of B(k) and $\delta(k)$. The pertinent properties of the primary standards used in this paper are listed in Table I.

The standards were powdered from crystals, uniformly diluted with vacuum grease, and placed in brass cells with Kapton windows. The total thickness was kept below the theoretical optimum in order to minimize thickness effects (26), since the signal-to-noise ratio was not a problem, and the powder size was made small enough that it would not introduce nonlinearities in the EXAFS (26).[2]

III. INITIAL DATA ANALYSIS

The procedures followed in data analysis were essentially those described in reference 12. Partial sums of the reaction center scans were performed, taking care to correct for shifts in the energy origin caused by jitter in the spectrometer. These partial sums and the total sums were analyzed separately to assess the errors due to random noise and systematic errors introduced in the analysis. The iron k-edge was isolated from the rest of the absorption by subtracting a smooth curve that was fit to the pre-edge data. The data were then normalized to unit edge step. The energy threshold E_0 was set to the peak (white line) at the top of the edge, and the data were interpolated from energy to k-space using $(\hbar k)^2/2m = (E - E_0)$. Another smooth curve was then subtracted to remove the smooth μ_0 background from the oscillatory EXAFS signal. Different background fits were generated and analyzed separately to assess systematic errors.

In fluorescence measurements, it is necessary to make corrections for the energy dependence of detector gains. The ion chamber that counts the fluorescence photons introduces no energy dependence, since it only counts photons of the fluorescence energy, E_f. However, the flux of photons incident on the sample is usually measured with an ion chamber that has a gain that decreases with the energy of the x rays because the chamber must be partially transparent. The fluorescence signals are divided by the measured incident photon fluxes. The decrease in the gain of the ion chamber with increasing energy thus somewhat exaggerates the measured EXAFS amplitude at high energy. For nitrogen fill gas in the ion chamber and the iron edge, the size of the effect on $\chi(k)$ is about 10% at $k = 8$ Å^{-1}. This would lead to slightly incorrect values of σ if it were neglected, unless the reference compound and the unknown were measured in exactly the same way. In the present case, corrections were necessary because the standards were measured in transmission mode and reaction centers in the fluorescence mode. The energy dependence correction is not required in the transmission mode because ln I/I_0 is evaluated to obtain μ. It should be mentioned that the intercepts (as opposed to the slopes) on a ratio plot are not changed appreciably by this correction, which approaches zero as k goes to zero. The effect is dealt with in a straightforward manner using absorption coefficients tabulated by McMaster et al. (27).

[2]E. A. Stern. Proceedings of the Daresbury Study Weekend on EXAFS for Inorganic Systems, March 1981. Davesbury laboratory report DL/SCI/R17.

IV. QUALITATIVE FEATURES OF THE EXAFS AND EDGE SPECTRA

Fig. 1*b* and *c* show the x-ray absorption spectra of 2Q reaction centers and of 2Q reaction centers treated with *o*-phen, both of which were prepared in our laboratory. The similarity of the spectra indicates that the environments of the Fe in the two samples are very similar. A quantitative comparison of the difference between the various spectra shows them to be the same within experimental error. *o*-phen evidently does not bind to the iron in the reaction centers. Fig. 1*a* shows the spectrum of the sample with two quinones and added *o*-phen that was prepared by G. Feher's group. The similarity to those in Fig. 1*b* and 1*c* is clear.

Near the absorption edge, details of the density of energy states and of the electron charge distribution around the absorbing atom strongly affect the absorption spectrum. The EXAFS, on the other hand, is relatively insensitive to such effects, so the two types of spectra are useful complements to each other. The edge spectra in Fig. 2*a* and *b* show that the charge distribution in the immediate vicinity of the iron atom in 2Q reaction centers is not appreciably affected by *o*-phen, in agreement with the spectra in the EXAFS region. The small differences between the spectra shown in Fig. 2*a* and *b* are due to differences in instrumental resolution. Spectra of the *o*-phen-treated sample and the control sample were virtually indistinguishable when they were measured simultaneously. The conclusion that *o*-phen does not bind to the Fe is strengthened by comparison with the edge structure of the Fe-*o*-phen chelate shown in Fig. 2*e*. The edge structure when Fe is chelated by *o*-phen is quite different from that of the reaction center. For most of the analysis described below we focused on the *o*-phen-treated sample, because it provided the highest signal-to-noise ratio.

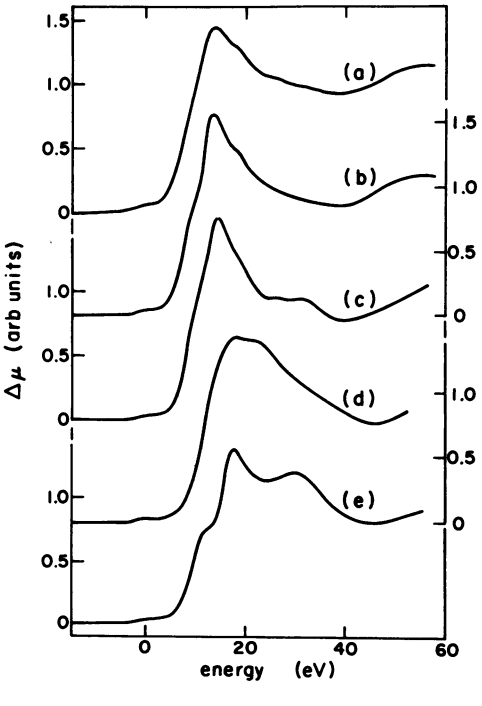

FIGURE 2 The near-edge structure of the x-ray K-edge of Fe in (*a*) two-quinone reaction center, (*b*) two-quinone reaction center with *o*-phen added, (*c*) an iron oxalate standard, (*d*) an iron glycine standard, (*e*) an iron(III)-*o*-phen standard. Iron(II)-*o*-phen had an essentially identical spectrum. The normalized spectra have been shifted in energy to approximately line up the 3d pips. Arbitrary (arb) units.

The small peak below the edge, which we call the "3d pip," is due to transitions to unfilled iron 3d states. These transitions are forbidden by the dipole selection rule but occur weakly due to quadrupole (28) and symmetry-breaking effects. Any lack of inversion symmetry of the iron environment allows odd parity states such as p states to hybridize with the d states, which in turn allows dipole transitions to occur in addition to the quadrupole transitions. The size of the 3d pip can thus be used as a measure of the strength of the odd part of the potential surrounding the iron. This is confirmed experimentally, as standards with tetrahedral iron coordination have 3d pips several times as large as those of compounds with octahedral coordination. For example, the oxide Fe_3O_4 has a spinel structure, in which two-thirds of the sites have octahedral coordination and one-third have tetrahedral coordination. The 3d pip is about twice as large in Fe_3O_4 as in octahedrally coordinated compounds (25, 29). This indicates that the size of the 3d pip in tetrahedral coordination is at least four times that in octahedral coordination.

The close similarity in size of the 3d pips in reaction centers and the octahedral standards (Fig. 2) indicates that the reaction center environment is approximately inversion symmetric, and in particular is not tetrahedral. This naturally suggests octahedral coordination, which is a preferred configuration for iron complexes.

The energy difference between the 3d pip and the peak of the absorption edge, which corresponds to transitions to the unfilled 4p states, is a measure of the distribution in space of electron charge transferred from the Fe to its neighbors. The larger the energy difference, the greater the charge transfer in the region between the radius of the 3d states and that of the 4p states. The splitting as measured from the onset of the 3d pip to the first peak past the edge is about 15 eV in reaction centers and in Fe(II) oxalate and 19 eV in the other standards (Table II). (The onset of the 3d pip is used instead of its peak because for some samples the peak is not well defined while the onset can be defined to within ~0.5 eV.) We conclude that reaction centers and Fe(II) oxalate have similar charge transfer distributions, as they have similar values for the energy splitting. In all the other standards, the degree of charge transfer is significantly larger.

It is readily apparent from the EXAFS data that the reaction center EXAFS phase is very close to that of ferrous oxalate (Fig. 3). This means that the average first-shell distance in reaction centers is close to that in

TABLE II
SPLITTINGS BETWEEN 3D PIP AND WHITE LINE FOR REACTION CENTERS AND STANDARDS

Standard	$E_{\text{white line}} - E_{\text{3d pip}}$
	(eV)
Fe-TIM	17.7 ± 0.5
Fe-*o*-phen	18.8 ± 0.5
Fe-glycine	19.8 ± 0.5
Fe-oxalate	15.6 ± 0.5
Two quinone reaction centers	
Prepared at Univ. of Washington	15.6 ± 0.5
With added *o*-phen	
Prepared at Univ. of Washington	15.6 ± 0.5
Prepared at Univ. of California, San Diego	15.1 ± 0.5

Fe(II) oxalate, which is 2.12 Å. The EXAFS oscillation of ferrous oxalate is of higher frequency than those of the other standards, indicating that the first-shell distance is larger in the former, in agreement with the known structures.

V. QUANTITATIVE ANALYSIS OF THE EXAFS SPECTRA

The close similarity of the edge spectra and the EXAFS phase in reaction centers and ferrous oxalate indicates that the oxalate is a particularly good standard for reaction center analysis. The accuracy in determining the types of neighboring atoms and their distances from the Fe atom in reaction center depends sensitively on the choice of the standard because of the relatively small range of k-space over which the reaction center EXAFS data are useful. The criteria for a good standard are many. One criterion is that sample and standard should have similar cutoff distortions so that the errors cancel. This requires that the nodes of the EXAFS oscillations in k-space should occur at the same values in the standard and reaction center so that the same window can be used for fourier transforming both spectra. Another possible source of error is the choice of the zero of energy used to convert from photon energy to k. If the standard and reaction center have similar near edge structure, both in shape and energy separation, then similar features in both can be used to set the E_0 at the same relative value. Even if the E_0 is off in an absolute sense, as long as the standard and reaction center suffer the same shift in their E_0 values, accurate distances can still be obtained. As pointed out above (and as discussed in more detail in section VI), similar near-edge structure indicates that the iron atom has a similar charge distribution in its vicinity for the two samples. This is important when one hopes to distinguish between N and O neighbors. Since the change in electronic charge between O and N is unity, a significant difference in the extent of charge transfer from the iron to its neighbors in the sample and standard can obscure the difference between O and N. Finally, corrections are required to the EXAFS formula, Eq. 1, because of the failure of the small-atom approximation (16). These errors are compensated for by using a standard that has the same Fe-to-first-neighbor distance as in the reaction center.

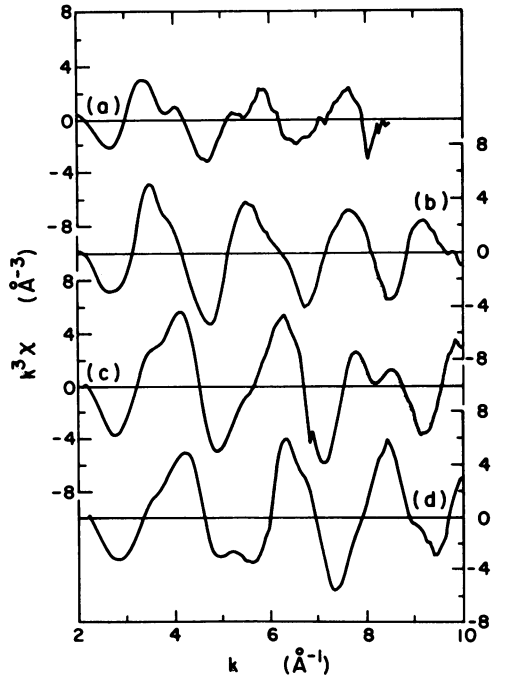

FIGURE 3 $k^3\chi(k)$ for (*a*) two-quinone reaction center with *o*-phen added (G. Feher sample), (*b*) an iron oxalate standard, (*c*) an iron glycine standard, (*d*) an iron(III)-*o*-phen standard.

The oxalate standard more closely satisfies the above criteria than any of our other standards. For that reason we did not use the usual procedure of directly comparing all of the standards with reaction center data and then interpreting the variations as estimates of the uncertainty in determining the structure around the Fe in reaction centers. We expect such variations because of the uncertainties mentioned above, which are introduced by the use of bad standards. The reaction center analysis was particularly susceptible to these variations because of the small k-range of its usable data.

We therefore used the following strategy to minimize errors introduced by poor standards. The oxalate standard was the only one directly compared to reaction centers. The oxalate standard, however, could be compared with our other standards since they all had useful data ranges substantially larger than reaction centers and thus were less susceptible to the problems listed above. The comparison was made by the ratio method discussed above. When the standards in Table I with the same nearest neighbors were compared with one another, the correct differences in nearest-neighbor distances were obtained to within about 0.01 Å, the amplitude ratio at $k = 0$ to within ~5% and the $\Delta\sigma^2$ to within ~0.0005 Å^{-2}. A difference in backscattering amplitude was discerned between N and O neighbors that was significantly larger than the variations between stan-

dards with the same neighbors. This gave us hope to distinguish between N or O neighbors in the reaction center. However, to do so we needed a good nitrogen standard comparable to the oxalate (oxygen) standard. As no such compound was available, we mathematically synthesized the amplitude of such a standard by multiplying the oxalate EXAFS $B(k)$ function by the ratio of the nitrogen to oxygen $B(k)$ functions, which were determined from the standards. Similarly, we added the oxalate phase to the difference of the empirical nitrogen and oxygen backscattering phases to generate the phase of the nitrogen "pseudo-oxalate."

Transformation into *r*-space

To determine the first-shell parameters precisely, we first isolate the EXAFS contribution of the shell from that of other shells. We do so by Fourier filtering the data (12). The EXAFS data are first multiplied by an appropriate window function and by k^3 to make the envelope approximately constant, and then are Fourier transformed with respect to $\exp(i2kr)$. For the reaction center data, the k range was generally 3 Å^{-1} $\leq k \leq$ 8 Å^{-1}. Extending the range to smaller k introduces distortions due to near-edge structure. The magnitude of the transform is shown in Fig. 4*a* as a function of r, which, to within an additive constant, is the distance from the Fe atom. The two main peaks are due to the first shell of ligands and a more distant shell; the bump at low R is due to residual background. Altering the size of the background bump by changing the background fit caused negligible changes in the first-shell and higher-shell signals, implying that the small residual background does not appreciably affect the structure determination.

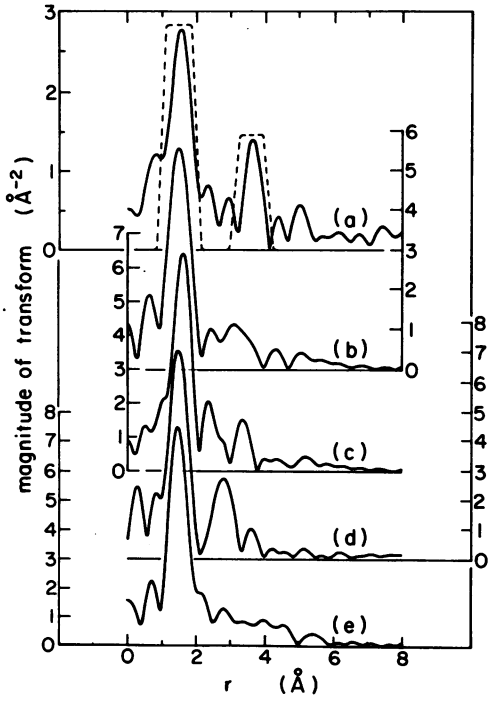

FIGURE 4 The magnitude of the Fourier transform of $k^3\chi(k)$ over the range 3 Å^{-1} $\lesssim k \lesssim$ 8 Å^{-1} for (*a*) two-quinone reaction center with *o*-phen added (G. Feher sample), and (*b*) Fe(II)-oxalate. The same Fourier transform but over the larger range 3 $\lesssim k \lesssim$ 10 Å^{-1} for (*c*) the same Fe-oxalate standard as in *b*, (*d*) an Fe-glycine standard, (*e*) an Fe-*o*-phen standard. In (*a*) the dotted lines indicate the region in *r*-space used to isolate and back-transform each peak into *k*-space.

It is interesting to compare the transforms of reaction centers with those of the standards given in Fig. 4*b–e*. The first-shell peak occurs at a somewhat greater distance for reaction centers and oxalate than for the other standards, as expected from the EXAFS phase. The size of the transform peak in reaction centers is also roughly half the size of the others. The more distant shell in the reaction center transform is most unusual. Most standards show no prominent structure that far out, and those that do have even larger peaks nearer to the first shell. The distant shell is too far from the Fe to be a second-neighbor coordination shell. Its peak is at ~3.8 Å; adding a phase shift correction of ~0.5 Å (see below) would locate it ~4.3 Å from the iron atom. Typical second-neighbor distances are from 3 to 3.5 Å. The relative size of the distant peak is larger than in the standard compounds, which is particularly surprising at such a large distance. It is clear that reaction centers have an unusual structure, and we shall analyze the distant shell in more detail below.

Isolation of the First Shell

We isolated the first-shell signal by multiplying the transformed data by a tapered, flat-topped window function, as indicated by the dotted lines in Fig. 4*a*, and then back-transforming the data within the window into k-space. Careful attention to window effects was essential in this analysis. Several slightly different windows were used to assess errors due to filtering. A flat-topped window minimizes the effects of small errors in window placement, and tapered edges reduce cutoff oscillations. Because of the finite window in r-space, the resulting Fourier-filtered data in k-space are somewhat distorted versions of the true single-shell data, but if they are compared with those of similar standard compounds treated with the same windows as discussed above, the distortions tend to cancel. This is one of the advantages of the ratio method. Because window distortions reduce the amplitude of the filtered data near the edges of the k-range, the ranges must be similar for the two compounds that one wishes to compare.

The properties of the standards used are listed in Table I. Standards with all-oxygen neighbors agree well with each other, as do the two standards with all-nitrogen neighbors. However, there are substantial differences between the all-oxygen and the all-nitrogen standards. This is illustrated in Fig. 5, where the natural logarithm of

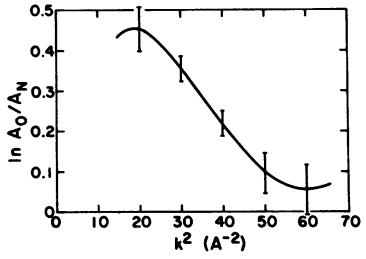

FIGURE 5 The natural logarithm of the ratio of the backscattering amplitudes of oxygen to nitrogen as determined from the standard compounds Fe-glycine and Fe-*o*-phen.

the amplitude ratio of an all-oxygen standard to an all-nitrogen standard is plotted vs. k^2. The standards used in Fig. 5 have the same number of neighbors and were corrected for their known structural disorders [i.e. multiplied by $(R_1/R_2)^2 \exp(2k^2\Delta\sigma^2_{structural})$]. The thermal disorder should be similar (since their chemical environments are similar, as judged by their edge spectra), so that the negative slope and the positive intercept must be due to the difference between the $B(k)$ functions of oxygen and nitrogen. Even if the thermal disorder is not the same for the two standards (as assumed), the intercepts would not be changed because any difference would simply cause the amplitude to be multiplied by $\exp(-2k^2\Delta\sigma^2_{thermal})$. Calculations of the backscattering amplitudes based on an independent-particle model (30) also give a positive intercept in a ratio plot over the same k range as used in Fig. 5, but the intercept is not as large as that measured. The theory is known to need substantial corrections for many-body effects.

The main difference between the nitrogen and oxygen $B(k)$ functions over the reaction center data range is not their overall sizes, which are similar for the two, but rather their shapes. The intercept obtained on the ratio plot appears to be particularly sensitive to the differences between oxygen and nitrogen. This is important because it provides a potential means of distinguishing nitrogen from oxygen ligands. However, caution is appropriate at this point. The intercept in the ratio plot will depend on the k-range used for the comparison. In comparing an unknown sample to a set of standards, it is important to use exactly the same k-range.

Because the near-edge spectra and EXAFS phase show that the oxalate standard and reaction centers have similar electron charge transfer distributions and first-neighbor distances, a comparison between the two eliminates errors introduced by the uncertainty in E_0, chemical effects, and breakdown of the small atom approximation. The ln-ratio amplitude plot vs. k^2 for the two is shown in Fig. 6*a*, and the phase comparison in Fig. 6*b*. The small phase difference (Fig. 6*b*) and the relatively small curvature of the ln-ratio amplitude plot (Fig. 6*a*) imply that the reaction center neighbors are either oxygen or atoms neighboring oxygen in the periodic table. From chemical knowledge, oxygen and/or nitrogen are most likely. The $k = 0$

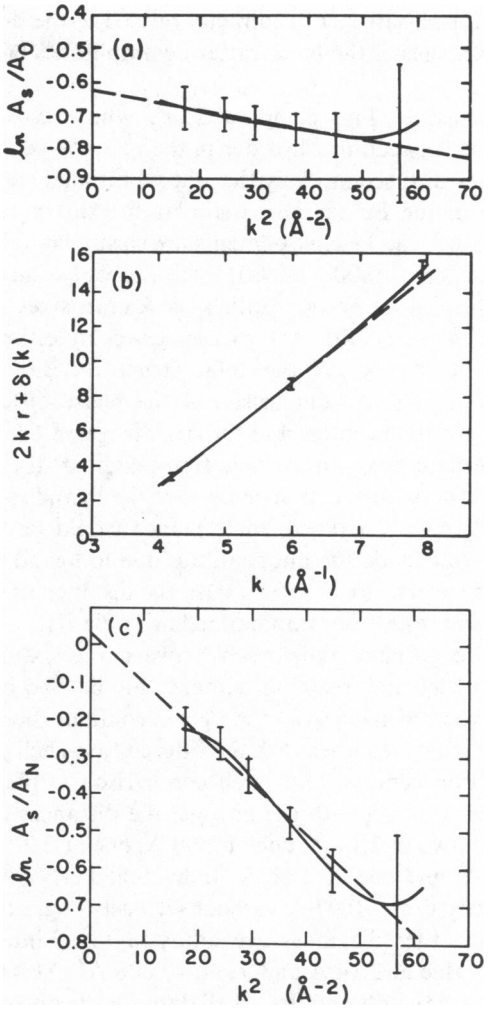

FIGURE 6 The natural logarithm of the ratio of the isolated first-shell EXAFS amplitude of the G. Feher reaction centers to that of (*a*) the six oxygens in Fe-oxalate and (*c*) six nitrogens in the same structural configuration as the oxygens in Fe-oxalate. The dashed lines are linear fits to the log amplitude ratio. (*b*) The phase of the oxygen EXAFS in Fe-oxalate (dashed line) compared with that of the isolated first-shell EXAFS of the G. Feher reaction centers (solid line). (Note offset zero in abscissa.)

intercept in Fig. 6*a* would translate into 3.2 ± 0.6 oxygen neighbors of the iron if there were only oxygen neighbors. The only integer consistent with this result is three oxygen neighbors, a result that is not reasonable. Even if the data were stretched to include four neighbors, the small size of the 3d pip eliminates a tetrahedral arrangement, leaving the unlikely possibility of a planar arrangement. We thus conclude that the Fe in reaction centers probably does not have only oxygen neighbors.

The standard with all-nitrogen neighbors mathematically synthesized in the manner described above is compared with the reaction centers in Fig. 6*c*. The $k = 0$ intercept in Fig. 6*c* gives the coordination number 6.2 ± 1.2, a result consistent with the presence of from four to six nitrogen neighbors, the rest being oxygens. The difference in coordination number in the two cases (3.2 for all-oxygen

and 6.2 for all-nitrogen) is directly related to the different k-dependencies of the backscattering amplitudes of O and N.

The slope in Fig. 6*c* gives $2\Delta\sigma^2$, where $\Delta\sigma^2$ is the difference between the disorder in the reaction center and the standard. It seems likely that the vibrational (thermal) disorder in the Fe oxalate is similar to that in reaction centers, since the Fe environments are so similar. Thus the measured $\Delta\sigma^2$ of 0.007 ± 0.001 Å^2 is probably due mainly to structural differences. Adding the known structural σ^2 of the oxalate (0.001 Å^2) to $\Delta\sigma^2$ gives an estimate of 0.008 ± 0.001 Å^2 as the total structural disorder of reaction centers. A comparison of the phase differences between reaction centers and the six-nitrogen model based on Fe oxalate gives an average first-neighbor distance of 2.14 ± 0.02 Å for reaction centers. If the ligands are four nitrogen and two oxygen, the distance would be 2.13 ± 0.02. If we include the uncertainties due to ligand type in the distance error bar, we estimate the distance as 2.14 ± 0.03. These results are summarized in Table III.

A more graphic comparison between the six-nitrogen ligand model and reaction centers can be obtained by plotting the predicted $\chi(k)$ for a given configuration of the nitrogen atoms together with the filtered first-shell $\chi(k)$ of the reaction centers. One such comparison is plotted in Fig. 7 for a model with the nitrogen-Fe distances distributed with two at 2.14 Å, one at 2.00 Å, one at 2.28 Å, one at 2.16 Å, and one at 2.12 Å. Individual Fe-N distances can be varied by ~0.07 Å without seriously degrading the fit if the other distances are adjusted to maintain the average value at 2.14 Å and σ^2 at ~0.008 Å^2. Also plotted in Fig. 7 are the filtered first-shell data for the uncorrected oxalate standard (four 0 ligands at 2.14 Å and two at 2.07 Å) to give a scale by which to evaluate the fit.

Isolation of the Distant Shell

Using a window function as indicated in Fig. 4*a*, the distant shell in reaction centers can be isolated in the same fashion as the first shell. A ln-ratio plot comparison of the distant shell and the first shell is given in Fig. 8. The linearity of the curve indicates that the distant shell is composed of atoms that have about the same atomic

TABLE III
PROPERTIES OF REACTION CENTERS WITH ADDED *o*-PHEN DETERMINED BY EXAFS

	Coordination number N	Mean distance	σ^2 (structural)
		(Å)	(Å^2)
1st shell*	6.2 ± 1.2	2.14 ± 0.02	0.008 ± 0.001
1st shell‡	5.2 ± 1.2	2.13 ± 0.02	0.006 ± 0.001
3rd shell	6.6 ± 2.6	4.3 ± 0.08	—

*Assuming six nitrogen atoms (see text).
‡Assuming four nitrogens and two oxygens.

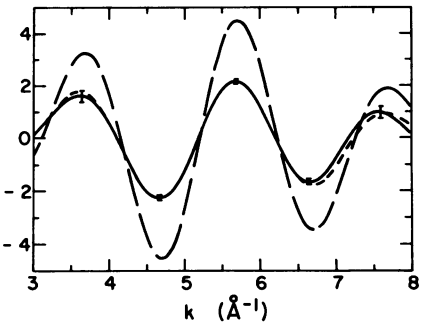

FIGURE 7 The fit of a model with six nitrogen ligands (short dashed line) to that of the isolated first-shell EXAFS of the G. Feher reaction center (solid line). The Fe-N distances in the model are given in the text. For comparison the isolated first-shell EXAFS of the Fe-oxalate standard is shown by the long dashed line.

number as those in the first shell, i.e., C, N, or O. If we interpret the slope as reflecting disorder, the distant shell has about the same disorder as has the first shell. The difference in distance between the shells is obtained from the difference in phase, which approximately equals $2k\Delta r$. The value of Δr determined this way is 2.18 ± 0.08 Å. This gives a value for the r_j of the distant shell of 4.32 ± 0.08 Å, as also listed in Table III.

Error Estimates

The errors can be divided into the usual random errors due to statistical noise and systematic errors that enter in the measurement and the analysis. The random errors and some of the systematic errors in the measurement were estimated by dividing the 13 scans into two partial sums of 6 and 7 scans. These partial sums were compared with one another and with the total sum, and errors were estimated from the fluctuations. The systematic errors in the analysis, which were the dominant errors, were estimated by reanalyzing the data using various slightly different analysis parameters (e.g., background fits and window functions). The errors also were assessed by testing the analysis procedures on synthetic data and on standards with known structures. It was of course necessary to do this using the same short range of k as was used for the reaction center

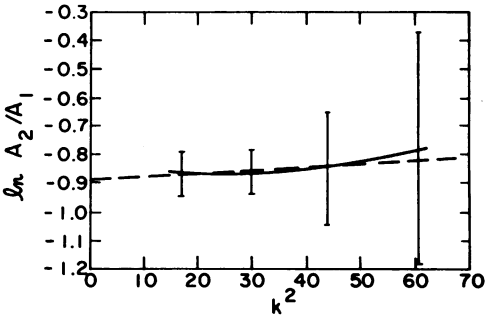

FIGURE 8 The natural logarithm of the ratio of the isolated distant-shell EXAFS amplitude to that of the isolated first shell in the G. Feher reaction center vs. k^2.

data. All error bars presented correspond to one standard deviation (60% confidence).

Errors due to uncertainties in the binding energy E_0 appear in the amplitude and phase of the EXAFS. To first order, an error ΔE_0 in the binding energy causes an error in the phase

$$\Delta\phi = -\frac{m\Delta E_0}{\hbar^2 k}\frac{\partial\phi}{\partial k} \simeq -\frac{m\Delta E_0}{\hbar^2 k}(2r_j + \delta_j'),$$

where δ_j' is the average value of $\partial\delta_j(k)/\partial k$ over the data range. Such an error influences the determination of the distance, r_j. The effect is potentially serious, because $\Delta\phi$ is largest at small k, where the useful data on reaction centers are concentrated. Fortunately, the uncertainty in the relative value of E_0 can be minimized by comparing reaction centers with Fe oxalate, which has a very similar near-edge structure. The uncertainty in the relative E_0 is ~2 eV, which gives an uncertainty of ~0.01 Å in the distance determination. Similarly, errors in the E_0 of this magnitude may be shown to cause errors in the amplitude intercepts of ~10%.

Additional complications can arise due to breakdown of the small-disorder approximation ($k^2\sigma^2 \ll 1$) that underlies Eq. 1. Large disorder can cause apparent shifts in the mean distance and errors in the estimate of σ^2. Fortunately, for reaction centers the disorder is not large in this sense, and analysis has shown that any such corrections are within our experimental error. In any case, these complications were circumvented by the fitting procedure, which models the actual radial distribution function. The success of the fit (Fig. 7) provides strong support for the initial analysis.

VI. DISCUSSION

The near-edge and EXAFS spectra are consistent with octahedral coordination of the iron by $(4 + n)$ nitrogen ligands and $(2 - n)$ oxygen ligands, where $0 \leq n \leq 2$. The near-edge structure clearly eliminates a tetrahedral environment, in agreement with the EXAFS. The most common bonding arrangement around Fe for oxygen and nitrogen neighbors is an octahedral one, and our data are consistent with such an arrangement. Butler et al. (9) have shown that the three axes of the Fe site in reaction centers are quite dissimilar from one another. This is consistent with the spread of distances and possible mixture of types of atoms in the first shell, which are responsible for the relatively rapid decay of the EXAFS amplitude with k.

The average Fe-ligand distance in reaction centers is similar to that in other ferrous high-spin Fe-N compounds (31, 32), and longer than in typical low-spin forms by ~0.1Å. The larger distance can explain why the ferrous form of reaction centers is stable relative to the ferric. The midpoint redox potential of the Fe has never been measured, but it evidently is above +0.45 V with respect to H^+/H_2 at pH 7. Electron paramagnetic resonance signals that reflect an interaction between the ferrous iron and a photochemically reduced quinone still occur if reaction centers are illuminated at this potential (D. Tiede and P. L. Dutton, personal communication). An isolated iron atom is most stable in the neutral state. Only when the iron is bonded to other atoms does its energy lower with transfer of charge. Quantum mechanically, the interaction occurs as the wave functions of neighboring atoms overlap one another. The shorter the distance, the larger the overlap, the stronger the interaction, and the greater the amount of charge transfer that occurs from the Fe to its ligand. Because the Fe in reaction centers has a large Fe-ligand distance, it is expected that a relatively small amount of charge transfer would occur.

The energy separation between the 3d pip and the edge as illustrated in Fig. 2 is a measure of the amount and distribution in space of the charge transfer from Fe. A direct experimental measurement of this dependence is afforded by optical spectra of various charge states of Co and Fe. Atomic Co is a more appropriate reference than Fe because the excited states of Fe observed in x-ray absorption correspond to a hole in the K shell. For these excited states the atomic core appears to have a nuclear charge that is one greater than Fe, and the states thus approximate the optically excited states of Co. However, transition metal atoms are similar, so that the results for Fe and Co do not differ greatly. Table IV lists values of the optical energy separations for both Co and Fe in various charged states (33). To correspond to the x-ray absorption values listed in Table II, these are calculated from the lowest energy term in the appropriate 3d configuration (corresponding to the onset of the 3d pip), and the average of the various energy terms corresponding to the 4p states that contribute to the peak just above the absorption edge. The third line gives a value for triply ionized Fe only, since data for triply ionized Co are not available. The 15 eV splitting in the reaction centers and Fe-oxalate corresponds approximately to removing two 4s electrons (Table IV), while the 18–20 eV splitting in the other standards corresponds to removing some 3d charge in addition to two 4s electrons.

A striking feature of the structure in reaction centers is

TABLE IV
OPTICAL ENERGY SEPARATION BETWEEN 3D ONSET TO PEAK OF 4P STATES*

Charge state‡	Co	Fe
	(eV)	*(eV)*
+1 (4s)	9.9	11.6
+2 ($4s^2$)	15.8	15.6
+3 ($3d4s^2$)	—	23.5

*C. E. Moore (33).
‡Terms in parentheses indicate electrons removed to produce charge state.

the prominence of the outlying shell at about 4.3 Å. The distant shell is too far from the Fe to consist of second neighbors. The invisibility of the intervening shells requires an explanation. Usually, in organic compounds containing a heavy atom, only the neighbor atoms nearest to the heavy atom are prominent in the radial distribution function obtained from EXAFS. The lack of visibility of the more distant atoms is caused by a combination of several factors in Eq. 1. One is the $[\exp(-2r/\lambda)]/r^2$ factor which attenuates the EXAFS more as r increases. Another is the larger structural spread in distances in the more distant atoms. Since the connection to the heavy atom is through intermediary atoms, variations in the bonding arrangement are cumulative with increasing distance. This factor is enhanced by the greater relative thermal motion of the more distant atoms. The nearest neighbors are directly bonded to the heavy atom, and thermal variation in their distance must excite the stretching mode. In contrast, a second nearest-neighbor atom is typically bonded to a first neighbor at an angle relative to the metal first-neighbor bond. A bending mode changing the angle will vary the distance between the center and the second-nearest neighbor atoms. Since a bending distortion is significantly less rigid than a stretching distortion, thermal excitations introduce much more disorder in distances to more distant atoms than to the nearest neighbors. In most organometallic molecules the Debye-Waller factor $\exp(-2k^2\sigma^2)$ of Eq. 1 induced by these two disorder factors will effectively suppress contributions of the more distant atoms.

There are three recognized mechanisms that can counteract these attenuation mechanisms and permit detection of distant shells by EXAFS. One is a symmetric, rigid structure around the iron. A porphyrin structure is an example of this sort. The geometric disorder is small because of the symmetry of the structure, and the rigidity keeps thermal disorder small enough to allow the detection of relatively distant atoms. However, the thermal disorder and the $r^{-2}\exp(-2r/\lambda)$ attenuation still increase with increasing distance. Thus, one expects intermediate atoms to be more prominent than the more distant ones, and this is verified by measurements on porphyrins (14). As noted above, the reaction center does not exhibit such behavior.

A counterbalancing effect occurs when the more distant atoms are heavy ones. The heavy atoms backscatter the photoelectron more strongly than the light atoms at higher values (30) of k, and their contribution is enhanced. An example of this occurs in the triiron compound "Fe glycine" (Fig. 3*c*). As determined in the preceding section, the distant shell in reaction centers is composed of low Z atoms, so the heavy-atom hypothesis cannot explain its prominence.

The third possibility is that the more distant atoms are collinear, or nearly so, with the first-neighbor atoms. The carbonyl group is an example. The collinearity helps in several ways. The thermal disorder is decreased since now only stretching modes are involved; and the intervening atom, by a quantum mechanical effect, focuses the photoelectron, enhancing the contribution of the outer atom to the EXAFS by a factor of ~3 (16). Since our data would require that the collinear group be composed of light atoms, the expected distance to the more distant atoms is 1.0–1.5 Å greater than the near-neighbor distance. However, the measured location of the more distant atoms is ~2.1 Å beyond the first neighbor. Thus, collinear atoms directly bonded together cannot explain our results.

The distant shell could be enhanced by approximate collinearity, even if it is not directly bonded to the first-neighbor ligands but is bonded through intermediate atoms. It still would have to be rather rigidly attached to the Fe ligands in order that the disorder not smear out its EXAFS. This suggests a ring structure connected to the iron ligands. The predominance of N in the first-neighbor ligands suggests a histidine ring. We have analyzed the expected EXAFS from a histidine ring attached through its ϵ_2 nitrogen to the Fe atom. In this model the two neighboring carbon atoms in the five-membered histidine ring are in the second coordination shell at a distance of 3.13 Å from the iron. The γ-carbon and δ_1-nitrogen of the ring are in the third coordination shell 4.27 Å from the iron, consistent with the measured distance for the distant shell. The third coordination shell atoms are approximately collinear with the N ligand, making an angle of 18.5° from exact collinearity; the same angle for the second shell from the histidine ring is 55°. Using the calculations of Teo[3] it is possible to estimate the focusing effects on the second and third coordination shell atoms in the histidine ring. The third shell has a large focusing enhancement factor of ~3, while the second shell has little enhancement. This is only an estimate of the enhancement, because Teo's formalism does not consider the numerous small contributions from multiple scattering by other atoms.

The factor-of-3 enhancement of the third shell relative to the second shell is decreased by the factor $(r_2/r_3)^{-2}\exp[-2(r_2 - r_3)/\lambda]$, where r_2 and r_3 are the distances of the second and third shells (Eq. 1). If one assumes that the Debye-Waller factor $\exp(-2k^2\sigma^2)$ is the same for the two shells, that the mean free path has the typical value of $\lambda = 6$ Å, and that a histidine ring contributes the same number of atoms to the two shells, the second-shell amplitude due to a histidine is expected to be 0.9 that of the third shell. Fig. 4*a* shows that the second shell amplitude, which should peak at about 2.7 Å, is <0.5 that of the third shell, which peaks at 3.8 Å. (Remember that the transformed peaks are displaced ~0.5 Å to smaller distances by the $\delta[k]$ term in Eq. 1.) Thus, to explain the reaction center results, an additional factor must further diminish

[3]Teo, B. K. Novel method for angle determinations by EXAFS via a new multiple scattering formalism. In press.

the second peak relative to the third. This factor could be the Debye-Waller factor.

X-ray analysis of small molecules containing histidine indicates that, to a first approximation, the histidine ring vibrates as a rigid body (L. H. Jensen, University of Washington, personal communication). An in-plane vibration of a rigid histidine ring pivoting about the first-shell N ligand produces about twice as much radial disorder in the second shell as in the third shell. This unusual result occurs because the third-shell atoms are more collinear with the Fe and the first-shell N than are the second-shell atoms. An in-plane rotation $\Delta\phi$ about the N ligand changes the distance between an atom in the ring and the Fe atom an amount $\Delta r = R\Delta\phi \sin\theta$, where R is the distance from the N ligand to the ring atom and θ is the angle between the line from the Fe to the ring atom and the line from the N to the ring atom. The larger R of the third-shell atoms is more than compensated by their smaller θ to produce a smaller Δr than for the second shell. The enhanced Debye-Waller factor in the second shell attenuates the EXAFS amplitude of the second shell relative to that of the third. Reasonable differences in the amounts of thermal disorder ($\Delta\sigma^2 \gtrsim 0.003$ Å^2) could decrease the amplitude to less than the required factor of 0.5.

A comparison of the relative amplitudes of the first and third (distant) shell is obtained from the plot in Fig. 8. Taking into account the different distances, the focusing enhancement of 3, and the mean-free-path attenuation, and assuming equal values of σ^2, we estimate that the third shell has ~1.1 times as many atoms as the first shell, or 6.6 ± 2.6 atoms. This corresponds to 3.3 ± 1.3 histidine rings attached to the six ligands around the iron, if we assume that other atoms in the third shell have a substantially larger σ^2 and are therefore invisible. The large error reflects the uncertainties introduced by the estimate of the focusing correction.

Recent amino acid analysis (34) indicates that the "L" and "M" protein subunits of the reaction center each contain five or six histidine residues. The Fe appears to be bound to one of these subunits (35). These numbers are consistent with the numbers of histidines around the Fe found here. Further support for the histidine ring explanation of the reaction centers EXAFS spectra is presented by recent EXAFS measurements on the metazido derivative of hemerythrin.[4] X-ray diffraction studies have shown that the two irons in hemerythrin are surrounded by five histidine rings, or two and a half rings per Fe atom (36). The Fourier transform to r-space of the EXAFS spectrum of this protein looks strikingly similar to that of reaction centers in Fig. 4*a*.

Our results show no indication that *o*-phen causes any significant disturbance in the structure out to the third coordination shell of the Fe. Because *o*-phen blocks electron transfer between the two quinones, this suggests that

[4]Elam, W. T., J. Loehr, and E. A. Stern. In preparation.

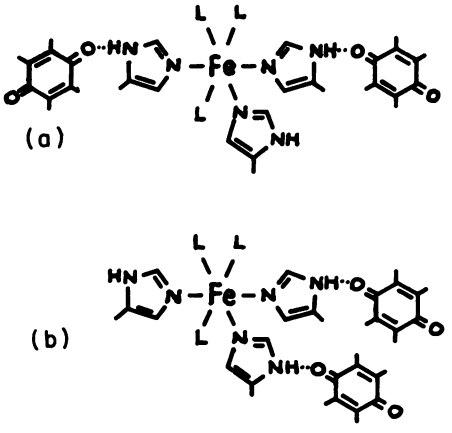

FIGURE 9 Possible arrangements of the two quinone to the histidine rings coordinating the Fe in reaction centers. (*a*) Quinones opposite side of the Fe. (*b*) Quinones adjacent.

the quinones are not directly liganded to the Fe. The sample from which one quinone was removed did show changes in its spectrum, but the interpretation of this is unclear because of the degradation of the sample. Other recent Mössbauer (35) and EXAFS (37) measurements also indicate that the quinones are not attached directly to the iron. One possibility is that the quinones are hydrogen bonded to histidine rings linked to the Fe. This possibility is schematically indicated in Fig. 9, with two possible arrangements of the quinones to one another. The quinones could be coupled to one another through the iron if they are linked to histidines on opposite sides of the iron, or they could couple to one another directly through histidines attached side by side on the iron. Valentine et al. (38) have discussed hydrogen bonding to histidines attached to Fe in heme proteins.

VII. CONCLUSIONS

Our measurements on the Fe site in reaction centers have clarified the structure of its environment. First, *o*-phen does not chelate the Fe. Its inhibition of electron transfer between the two quinones must result from some other effect. If *o*-phen disrupts the structure near the quinones, this disruption does not cause an observable change in the first three coordination shells of atoms around the Fe. This suggests that the quinones are attached more than two atoms from the iron. Further work should clarify this point.

The first-neighbor atoms of the Fe appear to be mostly nitrogens and are at an average distance of 2.14 Å, which is consistent with high spin ferrous Fe with nitrogen ligands. The most likely structure ranges from six nitrogen atoms to four nitrogens and two oxygens, all in an octahedral arrangement. The larger first-neighbor distance explains the stability of the ferrous form relative to the ferric form of reaction centers.

The mystery of the unusual prominence of the distant shell has been resolved by assuming that about three of the

first-neighbor nitrogen ligands are histidine nitrogens. This leads to an invisible second shell at 3.13 Å, and the prominent distant shell at 4.27 Å composing the third coordination shell. This interpretation is strengthened by the similarity of the EXAFS spectrum to that of metazidohemerythrin, which has 2.5 histidine ligands per Fe. We speculate that the quinones are attached to histidine ring nitrogens in the third coordination shell.

It should be emphasized that the distinction we have discerned between N and O is based on a limited k range. This required us to utilize exactly the same range of k space when comparing reaction centers with standards and has necessitated the mathematical synthesis of an appropriate nitrogen standard as described in the beginning of Section V. It is desirable to test the procedure against additional standards, and work of this nature is planned.

We have profited from many discussions with our colleagues, especially Lyle Jensen, Jon Herriott, George Feher, Mel Okamura, and Peter Eisenberger. The reaction sample used for our most detailed analysis and measurements was kindly supplied by George Feher. Thanks are due to Alma Johnson and Bev Dexter for their patient help in preparing the manuscript. The excellent support of the staff of Stanford Synchrotron Radiation Laboratory was essential in making our measurements.

The facilities at Stanford Synchrotron Radiation Laboratory are supported by National Science Foundation grant DMR77-27487. The research presented here was also supported by National Science Foundation grant PCM79-03674.

Received for publication 7 April 1981 and in revised form 21 July 1981.

REFERENCES

1. Feher, G., and M. Y. Okamura. 1978. Chemical composition and properties of reaction centers. *In* The Photosynthetic Bacteria. R. K. Clayton and W. R. Sistrom, editors. Plenum Publishing Corp., New York. 349–386.
2. Blankenship, R. E., and W. W. Parson. 1978. The photochemical electron transfer reactions of photosynthetic bacteria and plants. *Annu. Rev. Biochem.* 47:635–653.
3. Halsey, Y., and W. W. Parson. 1974. Identification of ubiquinone as the secondary electron acceptor in the photosynthetic apparatus of *Chromatium vinosum*. *Biochim. Biophys. Acta.* 347:404–416.
4. Vermeglio, A., and R. K. Clayton. 1977. Kinetics of electron transfer between the primary and secondary electron acceptor in reaction centers from *Rhodopseudomonas sphaeroides*. *Biochim. Biophys. Acta.* 461:159–165.
5. Blankenship, R. E., and W. W. Parson. 1979. The involvement of iron and ubiquinone in electron transfer reactions mediated by reaction centers from photosynthetic bacteria. *Biochim. Biophys. Acta.* 545:424–444.
6. Debus, R. J., M. Y. Okamura, and G. Feher. 1981. Dissociation and reconstitution of the H subunit from RCs of *R. sphaeroides* R-26. *Biophys. J.* 33:19a.
7. Parson, W. W., and G. D. Case. 1970. In *Chromatium,* a single photochemical reaction center oxidizes both cytochrome C_{552} and cytochrome C_{555}. *Biochim. Biophys. Acta.* 205:232–245.
8. Clayton, R. K., E. Z. Szuts, and H. Fleming. 1972. Photochemical electron transport in photosynthetic reaction centers from *Rhodopseudomonas spheroides*. III. Effects of orthophenanthroline and other chemicals. *Biophys. J.* 12:64–79.
9. Butler, W. F., D. C. Johnston, H. B. Shore, D. R. Fredkin, M. Y. Okamura, and G. Feher. 1980. The electronic structure of Fe^{2+} in reaction centers from *Rhodopseudomonas sphaeroides*. I. Static magnetization measurements. *Biophys. J.* 32:967–992.
10. Stern, E. A. 1974. Theory of the extended x-ray absorption fine structure. *Phys. Rev. B.* 10:3027–3037.
11. Lytle, F. W., D. E. Sayers, and E. A. Stern. 1975. Extended x-ray absorption fine structure. II. Experimental practice and selected results. *Phys. Rev. B.* 11:4825–4834.
12. Stern, E. A., D. E. Sayers, and F. W. Lytle. 1975. Extended x-ray absorption fine structure. III. Determination of physical parameters. *Phys. Rev. B.* 11:4836–4846.
13. Stern, E. A. 1976. The analysis of materials by x-ray absorption. *Sci. Am.* 234:96–103.
14. Cramer, S. P., and K. O. Hodgson. 1979. X-ray absorption spectroscopy: a new structural method and its applications to bioinorganic chemistry. *Progr. Inorg. Chem.* 25:1–39.
15. Stern, E. A. 1978. Structure determination by x-ray absorption. *Contemp. Phys.* 19:289–310.
16. Lee, P. A., and J. B. Pendry. 1975. Theory of the extended x-ray absorption fine structure. *Phys. Rev. B.* 11:2795–2811.
17. Stern, E. A., and S. M. Heald. 1979. An x-ray filter assembly for fluorescence measurements of x-ray absorption fine structure. *Rev. Sci. Instrum.* 50:4–7.
18. Jaklevic, J., J. A. Kirby, M. P. Klein, and A. J. Robertson, G. S. Brown, and P. Eisenberger. 1977. Fluorescence detection of EXAFS: sensitivity enhancement for dilute species and thin films. *Solid State Commun.* 23:679–682.
19. Okamura, M. Y., R. A. Issacson, and G. Feher. 1975. Primary acceptor in bacterial photosynthesis: obligatory role of ubiquinone in photoreactive reaction centers of *Rhodopseudomonas spheroides*. *Proc. Natl. Acad. Sci. U. S. A.* 72:3491–3495.
20. Tucker, W. F., R. O. Asplund, and S. L. Holt. 1975. Preparation and properties of iron(3+)-amino acid complexes. II. Crystalline complexes with aliphatic amino acids. *Arch. Biochem. Biophys.* 166:433–438.
21. Thundathil, R. V., E. M. Holt, S. M. Holt, and K. J. Watson. 1977. Preparation and properties of iron(III)-amino acid complexes. 2. The crystal and molecular structure of monoclinic tri-μ_3-oxo-triaquohexakis(glycine)triiron (III) perchlorate. *J. Am. Chem. Soc.* 99:1818–1823.
22. Burstall, F. H., and R. S. Nyholm. 1952. Studies in coordination chemistry. 13. Magnetic moments and bond types of transition metal complexes. *J. Chem. Soc.* 3:3570–3579.
23. Baker, J., L. M. Engelhardt, B. N. Figgis, and A. H. White. 1975. Crystal structure, electron spin resonance, and magnetism of tris-(*o*-phenanthroline) iron(III) perchlorate hydrate. *J. Chem. Soc. Dalton Trans.* 530–534.
24. Wyckoff, R. W. G. 1963. Crystal Structures. Wiley-Interscience Div. Series, New York. 5:416–417.
25. Heald, S. M., E. A. Stern, B. Bunker, E. M. Holt, and S. L. Holt. 1979. Structure of the iron containing core in ferritin by the extended x-ray absorption fine structure technique. *J. Am. Chem. Soc.* 101:67–73.
26. Stern, E. A., and K. Kim. 1981. Thickness effect on the extended x-ray absorption fine structure amplitude. *Phys. Rev. B.* 23:3781–3787.
27. McMaster, W. H., N. Kerr del Grande, J. H. Mallett, and J. H. Hubbel. 1969. Compilation of x-ray cross sections. Lawrence Radiation Laboratory Report No. UCRL-50174, sec. II. National Technical Information Service.
28. Bair, R. A., and W. A. Goddard III. 1980. *Ab initio* studies of the x-ray absorption edge in copper complexes. I. Atomic Cu^{2+} and $CU(II)Cl_2$. *Phys. Rev. B.* 22:2767–2776.
29. Shulman, R. G., Y. Yafet, P. Eisenberger, and W. E. Blumberg. 1976. Observation and interpretation of the x-ray absorption edges in iron compounds and proteins. *Proc. Natl. Acad. Sci. U.S.A.* 73:1384–1388.

30. Teo, B. K., and P. A. Lee. 1979. *Ab initio* calculations of amplitude and phase functions for extended x-ray absorption fine structure spectroscopy. *J. Am. Chem. Soc.* 101:2815–2832.
31. Katz, B. A., and C. E. Strouse. 1980. Spin state isomerism of tris(2-picolylamine) iron II. The diiodide and the hydrated dichloride. *Inorg. Chem.* 19:658–665.
32. Anderson, O. P., A. B. Kopelove, and D. K. Lavalle. 1980. Structure and properties of N-methyltetraphenylporphyrin complexes. Crystal and molecular structure and cyclic voltammetry of an air-stable iron II porphyrin: chloro(N-methyl-5,10,15,20-tetraphenylporphinato) iron II. *Inorg. Chem.* 19:2101–2107.
33. Moore, C. E. 1971. Atomic energy levels as derived from the analyses of optical spectra. *Nat. Stand. Ref. Data Ser., Nat. Bur. Stand.* 35:49–96.
34. Okamura, M. Y., G. Feher, and N. Nelson. 1982. Reaction centers in bacteria and green plants. *In* Photosynthesis: Energy Conversion by Plants and Bacteria. R. Govindjee, editor. Academic Press, Inc., New York. In press.
35. Debrunner, P. G., C. E. Schultz, G. Feher, and M. Y. Okamura. 1975. Mössbauer study of reaction centers from R. spheroides. *Biophys. J.* 15:226a.
36. Stenkamp, R. E., L. C. Sieker, L. H. Jensen, and J. Sanders-Loehr. Structure of the binuclear iron complex in metazidohemerythrin at 2.2 Å resolution. *Nature (Lond.)*. In press.
37. Eisenberger, P. M., M. Y. Okamura, and G. Feher. 1980. Investigation of the ferroquinone complex in reaction centers of *R. sphaeroides* R-26 by EXAFS. *Fed. Proc.* 39:1802.
38. Valentine, J. S., R. P. Sheridan, L. C. Allen, and P. C. Kahn. 1979. Coupling between oxidation state and hydrogen bond conformation in heme proteins. *Proc. Natl. Acad. Sci. U.S.A.* 76:1009–1013.